The Manufacture of Unbreakable Bionics via Multifunctional and Self-Healing Silk-Graphene Hydrogels

Kadumudi, Firoz Babu

2021-09

Kadumudi , F B , Hasany , M , Pierchala , M K , Jahanshahi , M , Taebnia , N , Mehrali , M , Mitu , C F , Shahbazi , M-A , Zsurzsan , T-G , Knott , A , Andresen , T L & Dolatshahi-Pirouz , A 2021 , ' The Manufacture of Unbreakable Bionics via Multifunctional and Self-Healing Silk-Graphene Hydrogels ' , Advanced Materials , vol. 33 , no. 35 , 2100047 . https://doi.org/10.1002/adma.2021000

http://hdl.handle.net/10138/346044
https://doi.org/10.1002/adma.202100047

acceptedVersion

The Manufacture of Unbreakable Bionics via Multifunctional and Self-Healing Silk–Graphene Hydrogels

Firoz Babu Kadumudi,[1] Masoud Hasany,[1] Malgorzata Karolina Pierchala,[1] Mohammadjavad Jahanshahi,[1] Nayere Taebnia,[2] Mehdi Mehrali,[2,3], Cristian Florian Mitu,[4] Mohammad-Ali Shahbazi,[5] Tiberiu-Gabriel Zsurzan,[4] Alireza Dolatshahi-Pirouz[1,2,6,*]

[1]Department of Health Technology, Technical University of Denmark, 2800 Kgs. Lyngby, Denmark.

[2]Department of Health Technology, Technical University of Denmark, Center for Intestinal Absorption and Transport of Biopharmaceuticals, 2800 Kgs. Lyngby, Denmark.

[3]Department of Mechanical Engineering, Technical University of Denmark, 2800 Kgs. Lyngby, Denmark.

[4]Department of Electrical Engineering, Technical University of Denmark, 2800 Kgs. Lyngby, Denmark.

[5]Department of Pharmaceutical Nanotechnology, School of Pharmacy, Zanjan University of Medical Sciences, Zanjan, Iran

[6]Radboud university medical center, Radboud Institute for Molecular Life Sciences, Department of Dentistry - Regenerative Biomaterials, Philips van Leydenlaan 25, 6525EX Nijmegen, The Netherlands.

*Correspondence should be addressed to Prof. A. Dolatshahi-Pirouz -aldo@dtu.dk.

Abstract: Electronic biomaterials capable of transmitting signals over longer distances than those typically encountered in rigid electronics are expected to open new opportunities for mankind by mimicking the way tissues propagate information. For seamless mirroring of the human body, they also have to display conformability to its curvilinear architecture, as well as recapitulate the mechanical capabilities of organs and tissues such as flexibility and self-healing. The union of soft and hard phases is a common nature-inspired approach for producing materials with advanced mechanical and electrical characteristics. In a similar vein, a facile strategy is developed herein for large-scale production of a multifunctional composite by mixing organic silk fibroin (SF) and inorganic reduced graphene oxide (rGO). The material was coined CareGum and capitalized on a phenolic glue - tannic acid (TA) – to facilitate sacrificial and hierarchical hydrogen bonds of varying strength with SF, TA and rGO. The hierarchal bonding scheme gave rise to high mechanical toughness, excellent conformability to arbitrary and complex surfaces, 3D printability, great electrical properties, as well as rapid self-healing and strong adhesion capacity. Indeed, the rGO reinforced silk exhibited a record-breaking elongation capacity close to 30000 %, elevated sensing sensitivity by 2-fold, 10-fold increase in electrical conductivity, and 4-fold increase in young modulus compared to its pristine counterpart. By taking advantage of these unique properties, we have for the first time developed a durable and self-healing bionic glove for hand gesture sensing and sign translation. Indeed, CareGum is a new advanced material with promising applications in fields like cyborganics, bionics, soft robotics, human-machine interfaces, 3D printed electronics, flexible bioelectronics, and point-of-care testing.

Silk fibroin extracted from Bombyx Mori (B. mori) cocoons is known for it's record-breaking specific tensile strength (~740 MPa), high toughness (6×10^4 Jkg^{-1}), good flexibility, and great resistance towards wear and tear from the environment.[1] The key factor behind these exciting properties stem from strong crystalline β-sheets and highly convoluted amorphous domains capable of dissipating mechanical energy within the fibroin backbone– a rare combination that is capable of uniting high mechanical strength and toughness coherently in the one and same system.[2] Their flexibility and softness enable them to integrate with the curvilinear and soft tissues, while their toughness can safeguard them from sudden mechanical failure after

integration into body parts that bear load and actuate. For this reason, silk-based materials have been used in flexible electronics for various Bionic devices such as cardiac sensors, brain electrodes electronic skin, and various biomaterial implants.[3]

Even though we have witnessed a growing interest in using silk-based electronics to interface between man and machine these approaches are still virgin attempts since they display properties in conflict with how the human body operates and our individualized anatomies. Additionally, besides being durable and resilient human tissues are also capable of undergoing self-healing when damaged; something that unequivocally counts as one of the biggest plusses in the evolution of biological systems. Indeed, without self-healing the survival mechanism of life would be significantly compromised; imagine just for one second living creatures combating diseases and injuries without their inherent healing capacity – ideally any man-made bionic device intended to interface indefinitely with human beings need to self-repair one-way or another. Electronics, going beyond just being conformable, soft and tough, but also embracing self-healing and ionotronics while taking advantage of the rapidly growing field of 3D printing have been prophesied as one of the key enabling technologies for addressing this grand challenge; as this beautiful marriage can yield unbreakable bionics with 3D printed personalized features.[4, 5] In simple terms, ionotronic devices operate by conducting electricity via ions instead of electrons like conventional electronics do.[5] Since tissues and organs are animated through complex ionic operations, ionic conductive materials can easily recapitulate the way electrical signals are mediated in living matter to yield electronics operating at the same time and length scales – this is important for manufacturing prosthetics bionics, and biorobots with human-like characteristics. In greater detail the operating principle here is based on ionically conductive materials that can adhere between metal-based electronics and living tissues to establish an intimate communication link between the realms of the animated and the inanimated; either directly, via another medium or through mechanical or electromagnetic transmittance. Unknown to many, silk-based materials besides their flexibility and mechanical toughness also exhibit capacity to conduct electricity via ions – something facilitated by water mediated proton-hopping from amino groups hidden deep within the peptide structure of fibroin and via possible ionic species in the medium.[6] They therefore could potentially position themselves at the very heart of the next-generation of soft electronic materials with the capacity to bridge the thick iron curtain still prevailing between machine and man.

The starting point of our journey begins by questioning our understanding of what a material is per definition and what it can do. Because what is lacking in this direction are hyper combinatorial materials covering a vast property portfolio including adhesiveness to metals and tissues, self-healing, sensing capacity, toughness, flexibility, stretchability, ionic conductivity, and moldability. Unlocking such secrets into the world of animated materials has captivated scientists for centuries dating back to the glory days of the alchemist, but at the same time it gives rise to critical questions regarding whether the proposed almost life-like materials even are feasible – can they exist – if yes can they be generated through economically efficient routes and become readily available for the broader populace? Indeed, a number of obstacles are standing against advances along this new and exciting avenue of material science. Because; how does one engineer a material with flexibility, toughness, strength, softness, adhesiveness, and electrical properties all in one without any unwanted tradeoffs? The story becomes even more combinatorial when self-healing and printability are added to this already wide portfolio of material properties. Turning the otherwise incredible silk from an ingredient of great materials of the past into our hypothesized winning material of centuries is not straightforward per say, and therefore never successfully attempted before. Even if the endeavor bode well, most material scientists would anticipate that the running line would only be reachable through a troublesome path and therefore not scalable and of use for society at all.

In the present communication, we have used inspiration from living tissues, to initiate a quest for the abovementioned silk material. In this uncharted territory, we identified a novel and scalable route for generating a **C**onductive, **A**dhesive, **R**econfigurable, and Visco**E**lastic gum (CareGum) with sensing capacity based primarily on silk - all through a non-toxic methodology devoid of any complicated chemical procedures. In simple terms; SF was mixed with Tannic acid (TA), calcium chloride ($CaCl_2$), and reduced graphene oxide (rGO) to facilitate the manufacture of a gum-like SiGo (Figure 1.a). Tannic acid (TA) is a polyphenol retrieved from bark and fruits from various plants and trees. It is also one of the most reactive small molecules in existence today because of a dendritic-like network of hydroxyl rich moieties such as pyrogallols and catechols. Notably, the active groups can mediate spontaneous self-healing based on hydrogen bonds with hydroxyl and amino groups. We also speculated - based on previous studies - that inclusion of $CaCl_2$ could play an important role in generating a CareGum with high toughness due to the electrostatic

interaction between positively charged calcium (Ca^{2+}) ions with negatively charged groups in the SF backbone.[7, 8] Graphene on the other hand display formidable electrical (sheet resistance ~30Ω □$^{-1}$),[9] thermal (withstand up to ~1000 ºC)[9] and mechanical properties (130 GPa, tensile strength)[10] 200 times stronger than that of steel while being ionically active at the same time;[11] something that arises from a unique 2D honeycomb structure. It has therefore been utilized in a wide range of fields e.g., biomedical engineering, electronics, energy harvesting and storage, sensors and composites and coatings.[12] Here, we have explored the impact of different SF – rGO ratios (from 0 to 20 wt% nanomaterial loading) on the self-healing, adhesiveness, mechanical, sensing and electrical properties of SiGo; while keeping the constant weight ratio of SF:TA at 1:5 and 0.1 M $CaCl_2$. The CareGum was not entirely a hydrogel, neither was it completely solid, indeed it was more reminiscent of something in between – almost like a gum - with a water content decreasing from 47% to 36% as the rGO concentration reached 20% (Figure 1b). The cross-sectional scanning electron microscopic (SEM) images of the CareGum shows microporous structure with 2-3 μm pore size, whereas an increased pore sizes with 5-10 μm pore size were observed with rGO incorporation due to the formation of wall boundaries around the pores by stacking of rGO layers (Figure 1c). Nevertheless, these increased pores does not contribute to hold a large amount of water in the cross-linked networks. The lower water uptake in the composites could be attributed to the hydrophobic nature of the rGO.

The investigations were complemented by chemical characterizations through Attenuated Total Reflectance- Fourier-Transform Infrared (ATR-FTIR) spectroscopy. As shown in the Figure 1d, the FTIR spectra of CareGum samples exhibit prominent signature peaks associated with silk (amide I (1642 cm^{-1}), amide II (1515 cm^{-1}), amide III (1235 cm^{-1})) and TA (C=O stretching (1698 cm^{-1}), C-C stretching (1609 cm^{-1}), C-O-C stretching (1308 cm^{-1})), as expected.[8, 13] Specifically, the composite showed a wavenumber shift of the TA associated hydroxyl group (OH) centered at 3400 cm^{-1} and the amide (NH) associated peak of silk centered at 3290 cm^{-1} to 3323 cm^{-1}. These shifts indicate the presence of a multitude of hydrogen bonding schemes between TA and SF of varying strength ranging from OH_{SF}….OH_{TA} (4.7 kcal/mol), NH_{SF}….OH_{TA} (7.4 kcal/mol), and OH_{TA}….$C{=}O_{SF}$ (4.6 kcal/mol).[14] In addition, the peak at 1698 cm^{-1} corresponding to the carbonyl group (C=O) of TA is shifted to 1713 cm^{-1}

confirming the weak interaction between silk and TA through NH_{SF}….$C{=}O_{TA}$ (3.9 kcal/mol) hydrogen bond formation. From FTIR we can also examine possible electrostatic interactions between positively charged calcium (Ca^{2+}) ions with negatively charged amino acids (COO^-) such as glutamate and aspartate within the SF chain.[7, 8] This interaction did not make a significant change in the peak position of amide peaks, howbeit a decreased intensity of the amide I (1642 cm^{-1}) and amide II (1515 cm^{-1}) of SF were observed, which according to the literature typically are associated with structural changes occurring in the backbone of the SF chain via the abovementioned electrostatic interactions with Ca^{2+} ions. [7, 8, 15]

Further, to improve the conductivity of the CareGum, rGO was incorporated in the composites. Here we employed a green approach to reduce GO by using TA for the chemical reduction process and it will help to modify rGO surface with TA through π-π interactions, which also benefits in better dispersion of rGO in the composites. In the FTIR spectrum of rGO, the oxides peaks from rGO disappeared and displayed signature peaks from the TA, which confirms the reduction and modification of rGO surface with TA (Supporting information, Figure S1). Therefore, the peaks corresponding to rGO were merged with SF and TA related absorption peaks. However, there is a decrease in intensity corresponding to the amide I and amide II bands within the SF spectra were observed after rGO inclusion (Figure 1d, enlarged spectra)[8, 16]. This additional decrease in intensity could be attributed to possibly conformational changes occurring in the secondary structure of SF due to surface interactions with rGO. We expect that these conformational changes in the molecular level of SF could impact mechanical properties such as toughness and stiffness. Therefore, we deconvoluted the amide I spectra in the 1571-1800 cm^{-1} region to elucidate the secondary structures present in silk (Supporting information Figure S2). From this analysis, we unraveled four of these including β-sheets, random coils, α-helices, and β-turn structures.[8, 16] β-sheets are crystalline structures formed by interpeptide antiparallel hydrogen bonded strands – something linked to material stiffness and toughness - while β-turns arise from the transformation of loose hairpin structures into tight turns and typically associated with an increase in sample elasticity.[16, 17] As you can see in Figure 1b, the addition of TA and $CaCl_2$ increased the β-sheets and β-turn structures (together 42%) compared to pristine silk (22%) and SiGo without $CaCl_2$ samples (30%) – this could possibly increase the toughness of the

CareGum. The mechanism of β-structure formation could be explained by Ca^{2+} ions disrupting hydrophobic interactions and salt bridges between adjacent SF chains via charge shielding and instead facilitating a conformational transition of random coils to more ordered β-structures.[7, 8] Interestingly, the nanoreinforcement of CareGum with graphene further increased the percentage of β-structures to 49% at the highest rGO concentration. As reported previously, the interface of 2D materials can induce conformational changes from random coils and α-helices to crystalline β-structures through surface facilitated polypeptide chain folding. Differential Scanning Calorimetry (DSC) analysis provided even more insights into the intimate structure of the CareGum matrix, as this methodology mapped out various phase transitions in SF related to glass transition (Tg), crystallization and thermal degradation point (Supplementary Fig. S3). To this end, pristine SF showed a glass transition (Tg) behavior around 178 ºC. The addition of TA and $CaCl_2$ increased the glass transition behavior to 190ºC – a possible indicator of intensified interactions between SF and TA facilitated through more hydrogen bonds. Similarly, the non-isothermal crystallization of the SF amorphous chain at 227 ºC increased to 231 ºC due to the restricted movement of SF chains caused by the strong interaction between TA with SF. The inclusion of rGO did not display a significant impact over Caregum thermal properties and only slightly increased the Tg-value with three degrees to 193 ºC.

In summary, the many exciting self-healing and mechanical CareGum properties that we will soon bear witness could arise from the hierarchical bonding scheme between SF facilitated by Ca^{2+}, TA and rGO and consisting of hydrogen and electrostatic bonds with varying binding strengths. In this scheme, the weak bonds are reversible and thus self-healing, while simultaneously enabling an avenue for dissipating mechanical energy to avoid stress buildup and sudden mechanical failure. This all together can give rise to high toughness and self-healing properties. The electrostatic interactions between SF with TA is also a complementary avenue for dissipating energy since such bonds are reversible as well, but Ca^{2+} inclusion can also intensify β-structure formation rate as described above and thus increase mechanical toughness.

As mentioned previously CareGum is a highly stretchable material capable of rapid self-healing while displaying the ability to become molded into complex shapes and architectures with ease (Supplementary figure S4 that shows this). This is

demonstrated in Figure 2.a. Here two pieces of CareGums are gently pushed together to examine self-healing capacity. Indeed, after only a few minutes the individual pieces merged into one CareGum that could stretch homogenously along its x-axis (Figure 2.b). Notably, CareGum readily molded into a ring almost like play-dough and could elongate to around 240 times its original length after healing. The rapid healing process is examined in greater detail in Figure 2.c through optical images acquired at different time-points in combination with scanning electron microscopy (SEM) images (Figure 2.d). The self-healing properties were scrutinized further in Figure 2.e through compression testing before (pristine) and after healing at both 25 and 37 degrees. These results demonstrate that CareGum could heal with 95% efficiency after 1 min. The trend was pretty much the same at both temperatures.

In recent years, smart electronic textiles have emerged as promising healthcare monitors for continuous health tracking and human-machine-interfacing via Bionics as they are capable of blending with the patient's anatomy without any discomfort.[18] Most of these functionalities were achieved on textiles through embedding rigid electronics within them. Unfortunately, an inherent mismatch between heaviness/rigidity and flexibility/lightweight has until now compromised the durability, patient comfort and aesthetic appearance of such devices. Here, we attempted to produce electronic and self-healing fibers with CareGum that potentially can become embroidered into smart textiles in a seamless manner making them more durable and comfortable to wear for the user. To this end, a simple melt spinning process at 60 ºC was employed to transform the CareGum into fibers with millimeter sized diameters via extrusion through a syringe nozzle (Figure 2f). In brief, during heating the reversible hydrogen bonds between SF and TA breaks, thereby reducing the bulk viscosity making it more liquid-like and easier to extrude. This process does not require any additional pre-treatment or post-treatment like other hydrogel wet spinning techniques, indeed compared to their conventional counterparts a rapid cooling to room temperature produced very smooth fibers. The flexibility and weaving ability of the CareGum melt spun fibers are demonstrated in the Figure 2f To this end, we showed that they were readily twistable into cable-like structures and could interlace into woven-like textiles (supplementary figure S5) – importantly they could self-heal within seconds if damaged. In summary, we have demonstrated that the Caregum can give rise to thin self-healing fibers via melt spinning; something

which potentially can open a new additive manufacturing window for producing 2D and 3D soft woven structures with combinatorial material properties.

Soft ionotronics typically utilize sophisticated communication bridges between biological systems such as the human body and polymers/metals; something typically facilitated by adhering soft ionic conductors between them, via a dielectric medium and sometimes with the aid of mechanical or electromagnetic transmission. Given the abundant catechol groups on TA and reactive hydroxyl groups on rGO we hypothesized that SiGo could adhere to a wide range of surfaces ranging from tissues, polymers to metals by mimicking a mussel adhesion mechanism.[19] In Figure 2.d-e we have tried to uncover this exciting property by initially using a simple gravity-based test wherein the Caregum was sandwiched between a 100 g weight and various surfaces including glass and porcine skin. These images clearly demonstrate its incredible gluing property as the CareGum could stretch to 15 times without becoming structurally unstable, while facilitating a strong surface adherence after the weight was in free fall mode. We then made use of lap shear testing (Figure 2.f) to quantify the adhesiveness of CareGum to both tissue, metal and glass interfaces. In most of these curves we observed a gradual peel-off process with a long stripping lag phase; something reminiscent of a robust adherence mediated through a balanced contribution of adhesion and cohesion (supplementary figure S6). The results have been quantified and displayed in Figure 2.g.-h. From here it is evident that the shear stress needed to facilitate adhesive failure increased dramatically as a function of rGO concentration on brass and stainless; while it was fairly rGO-independent on Glass. Specifically, the highest adhesion strength was found on brass ranging between 48 – 144 kPa (0 to 20%) and the lowest on glass (50-58 kPa) and Poly (methyl methacrylate) (PMMA) (10-19 kPa). On the other hand, the adhesion strength on skin, muscle, and heart was pretty much unaffected by the rGO concentration. Here, the highest adhesion strength was determined for skin ranging between 16.6-18.6 kPa and the lowest on muscle and heart ranging between 3.7-5.5 kPa and 4.0-5.0 kPa; respectively. We speculate, that the strong adhesion to skin is caused by possible hydrogen bonds with OH-groups available on keratin and ceramides in the outermost layers of skin and OH-groups from rGO and TA.[20] Indeed; almost 20 % of the skin is made from the hydroxyl rich amino acids proline, glycine and hydroxyproline.[21] On brass and stainless steel the interaction could possibly be mediated by electronic or

van der wall interactions between rGO and the metal surfaces;[22] befitting the observed link between adhesion strength and rGO concentration in Figure 2g-h.

Native-like mechanical properties are crucial for securing durable and native-like integration with living and mechanically active tissues including bone, cartilage, muscle and heart. In a worst-case scenario a mismatch can facilitate scar tissue formation ultimately leading to device failure. This prompted us to carry out a series of mechanical tests beginning with tensile testing (Figure 3.a). From here a formidable extension capacity is demonstrated close to around 30000 % for some of the samples - almost three-fold larger than the current record at 10000 %.[23] In this study the authors doped the backbone of (dimethylsiloxane) (PDMS) with pyridinecarboxamide (pdca) to establish a coordination complex mediated by Fe^{3+}. In doing so they also managed to make the PDSM self-healing; albeit at a much lower rate than what is observed in Figure 2. In comparison standard sylgaard 184 PDMS can only elongate 200 % before rupturing, while other elastic polymers including SEBS and polyurethane break at 700 % and 280 % strain, respectively.[24] The observed stretching property for the CareGum material increased from 20500% (toughness: 8.9 ± 1.1 MJ m^{-3}) to 24000 % (toughness: 9.9 ± 1.9 MJ m^{-3}) with 10% rGO incorporation and then dropped to 15500% (toughness: 13.9 ±2.2 MJ m^{-3}) for the highest rGO concentration, while the tensile strength seemed unaffected by rGO (Figure 3.b-c). This phenomenon is widely encountered in the field of nanoreinforced soft materials and typically caused by mechanical stress build-up and the associated devastating energy burst release from nanomaterials sliding over one another almost in a similar vein earth quakes are generated from friction between tectonic plates. On the contrary a sharp three-fold increase in compressive strength from 287 to 820 kPa is seen as the rGO incorporation increased to 20% (Figure 3.d). Likewise, the young modulus increased four-fold from 5.7 to 21.7 MPa. We expected this due to the reported formidable mechanical properties of graphene– and the fact that it becomes fully exploited in compressive mode as the rGO-rGO spacing dramatically decreases here ultimately enabling the hard phase of the CareGum to outcompete the soft phase. Similarly, an intimate link between rGO concentration and energy dissipation was discovered in Figure 3.d. To this end, a rGO concentration change from 0 $\rightarrow$ 20% increased the energy dissipation from 0.29 $\rightarrow$ 0.61 MJ/m^3 (Figure 3.d). Notably, after the first cycle we observed a fairly cyclic behavior at 30 % with almost 16%

hysteresis for SiGo-0% and 22% hysteresis with SiGo-20% from cycles 2 → 4. This slight increase in hysteresis with rGO incorporated samples may be due to the loss of energy by friction. To improve the cyclicity of our silk-inspired CareGum even more we embedded it within a 3M VHB-tape and ran the same number of cycles as before but this time up-to 600 % strain. Here, smaller energy dissipation ranging from 0.09-0.085 MJ/m^3 (2→ 4) was observed with only 5% hysteresis. The results in Figure 3 therefore paint a promising picture of a mechanical durable material befitting the many demanding environments of the human body.

Next, we carried out electromechanical tests to examine the relation between electrical resistance and mechanical deformations involving stretching, bending and twisting (Figure 3e). To measure the resistance changes, both ends of the CareGum strips (30 x 5 x 1 mm) were connected to a tin plated copper foils and then embedded within a 3M VHB tape to improve their recovery. Then, CareGums were stretched up to 600% strain while we examined the relative resistance changes ($\Delta R/R_0$, where $\Delta R = R-R_0$, R is the change in resistance and R_0 is the initial resistance) as function of strain. Notably. when compared to other CareGums, a lower hysteresis was observed with SiGo-20% due to its high elastic nature after rGO incorporation (Supplementary figure S7a). We therefore decided to rely solely on this composition in the following electromechanical bend and twist tests. To this end, we observed that the relative resistance change for SiGo-20% only increased with 12 % twisting after four twists and 19 % after bending (angle between 1-180^o). We can thus confidently conclude that CareGum is a really durable sensor even when undergoing extreme mechanical deformations. Overall, the results highlighted here demonstrate that the CareGum is a promising component for flexible electronics - especially in wearable applications where the monitoring of multidirectional body movements without loss of electrical functionality is required

Even though, a low resistance change ($\Delta R/R_0$) per strain – referred to as gauge factor (GF) – bodes well for flexible electronics that needs to remain electrically active during the extreme shear strains typically encountered in disruptive technologies including bendable displays, electronic-skin, soft robotics and origami electronics. On the other hand; if the GF-value becomes compromised the sensitivity drops. To make ends meet; strain-gauge sensors were GF and resistance drop are fairly balanced are thus highly desirable in the field. Typically, highly stretchable and

self-healable soft hydrogels show very low GF compared to brittle strain sensors. For instance, the values reported for metal-based strain-gauges are around 2.0, however they can sustain only very small strains up to 5%, whereas the soft hydrogels are extendable in the range 100-1000% with GF-values between 0.125 – 1.6.[25] Hydrogel-based sensor is thus carving a new exciting path in the field compared to their conventional metal-based counterparts. In this direction, our stretchable CareGum material showed a comparable GF = 0.5 at 100% strain, increasing to 0.64 at 600% strain. The inclusion of 20 % rGO showed a lower GF value below 300% (GF= 0.31 at 100%), however it significantly improved above 300% reaching GF = 1.04 at 600% (Supplementary Figure S7b). The inclusion of rGO therefore improved the mechanical strain-sensitivity by almost two-fold.

Biomechanical sensing have open up for novel opportunities in continuous healthcare monitoring covering diseases in which parameters such as swelling, actuation, strain and movement play an important role.[26] Traditionally, this forum has been based on technologies ranging from various capture imaging setups to electronics consisting of gyroscopes, magnetometers and accelerometers.[27] The later is an enabling technology and currently driving the engine in the field of wearable electronics, but at their very heart a number of limitations such as rigidity issues, high-cost, low-sensitivity and non-durability still prevails. Strain-gauge sensors such as the CareGum can obliterate the challenges in this direction by electrically linking to human biomechanics via mechanical vectors. In addition they also encompass the wide range of properties required to enable proper integration with the body in combination with high sensing sensitivity contrasting the current mono-functional sensors out there. In supplementary Figure S8 we have demonstrated that CareGum-based sensors can capture a wide range of human-motion sensing including movements of various joints, facial expressions and hand gestures. Advantageously, higher amplitude movements resulted in larger ($\Delta R/R_0$) and were thus measurable – same goes with speed, as faster movements gave riser to more closely spaced amplitude peaks. Speed is traditionally measured with complex and delicate components in the existing sensors on the market, whereas the CareGum sensor captured this feature with higher fidelity through a much simpler and cheaper methodology based on strain sensing.

We foresee that the CareGum because of the described moldability in Figure 2 can become useful in customized biosensors capable of melding with patient-specific details and individual anatomies. In combination with 3D printing we envision the possibility of on-site manufacturing of personalized sensors to target a wide range of diseases in greater detail. A key requirement in this direction is shear-thinning capacity. Such materials are easily extruded through an extrusion needle in response to proper shear force. For this reason, we performed rheology testing on CareGum. Our first observation was that the material was not extrudable at room temperature. However; the storage modulus of CareGums incorporating 20 % rGO dropped dramatically with increasing temperature reaching 32 kPa at 50° (Figure 4.a); notably this behavior was cyclic and therefore the CareGum also yield mechanical thermoreversibility. This prompted us to examine the relation between material viscosity and shear-rate at 50°. The results clearly show an intimate link between the two with the viscosity reaching around 200 (Pa.s) from 2000 (Pa.s) at 100/sec shear rate a value matching what a material typically will experience when manually being pushed through a 22 gauge needle (Figure 4.b). Noteworthy, (100 Pa.s) is typically considered flowable since the viscosity of honey is 10 (Pa.s) and that of Peanut butter is 250 (Pa.s) for sake of comparison. Indeed, we expected that sacrificial and self-healing bonds such as those present in SiGo would give rise to shear-thinning properties due to the observed fast self-healing recovery in Figure 2.

We next examined the fluid mechanical properties of the CareGum as a function of rGO content (Figure 4.c). At 0 % rGO CareGum behaved like a pseudoplastic fluid, but at higher rGO content the behavior turned into something more reminiscent of a Newtonian fluid. We speculate, that the transition from a parable-shaped non-Newtonian fluid to a more linearly one is in reality marking a transition into the realm of shear-thickening materials (Dilatants) – since Dilatants are famed for the ability to increase their mechanical properties in response to shear rate.[28] This property shields them against sudden mechanical shocks and the observed trend in this direction correlates well with a number of recent studies demonstrating that nano and micro materials hold the secrets of shock-absorbing fluids. We anticipate that even higher rGO concentration could potentially give rise to such properties in the CareGum as well, however, it was unfortunately not possible to load the CareGum with more rGO.

In Figure 4.d we have utilized the unique rheological properties of the CareGum and molded it into complex shapes and in Figure 4.e we have shown that it can conform on the curvilinear shape of a human finger and follow it during various bend-related movements. The impressive configurability of CareGum encouraged us to build soft and self-healing electronic circuits of varying complexity by using an in-house-built pen-dispenser (Figure 4.f). Briefly, we are able to illuminate a LED lamp connected to the deposited circuits. As a next step, we dispensed a simple linear circuit with electrical self-healing capacity (Figure 4.g) and showed that it is capable of illuminating a LED lamp. As expected, once the soft circuit is cut into two pieces the conductive drops and consequently the LED stops glowing. Advantageously, the circuit quickly healed both electrically and mechanically, as evident from the LED intensity and the high stretching capacity of the healed circuit. This is more clearly demonstrated in Figure 4.g, wherefrom we have calculated en electrical recovery time at 60s. Notably, the circuit could recover cyclically as evident from Figure 4.f. Finally, in Figure 4.h we have tried to capture the relation between conductivity and rGO content. From here a sharp 10-fold increase from 1 x 10^{-3} to 1 x 10^{-2} S cm^{-1} is observed as the rGO content varied from 0 to 20%. Despite the reported moderate CareGum conductivity it still surpassed values typically seen in tissues; indeed cerebrospinal fluid – a tissue holding the highest conductivity in the human body - display a value appreciably lower than the CareGum at around 15 x 10^{-3} S/cm.[29]

We finally utilized the unique rheological properties of CareGum to custom print various designs with a number of well-established printing technologies. First, we used screen-printing, which is a simple method for creating complicated patterns based on a screen pattern transfer technique, in which a negative screen with the desired pattern is placed against a print substrate. In brief, by heating the CareGum up to 60 ^{o}C it started to flow - almost in a honey-like manner – and thus was easily pushed through the negative screen and onto the substrate in complex designs (Figure 4.i-j). The methodology showcased in Figure 4 is an elegant forerunner towards the final goal of customized wearable electronics that can capture personalized information much better than its predecessors. In this vision of ours, the personalization is established by custom-printing the electronics in desired circuitries matching the targeted tissue. Specifically, in this scenario, 3D extrusion printing technology can be combined with scanners to yield biomechanical sensors that can connect with pivotal locomotion points within the patient's body. We have

demonstrated the capability and feasibility of the 3D printing of CareGum materials by utilizing a thermal-assisted extrusion technique. To achieve this, wet samples of SiGo-20% samples were loaded into a steel syringe with a plunger mounted to a heating element. The syringe were heated up to 40 ºC and slowly extruded (speed 18 mm/min) through a nozzle with a diameter size of 2mm. Figure 4 j shows the various complex 3D printed structures including spiral, square, cube, pyramid, and cylinder. It is also evident that the 3D printed structures of SiGo-20% were strong and elastic enough to support its own weight. The fast self-healing ability of the CareGums was a greater advantage here, which helped to heal the layers very quickly to form the 3D stacks.

Building on these results we have generated an electronic glove (E-glove) that is capable of monitoring complex hand movements; something useful for improving surgical dexterity of surgeons, recreational virtual gaming, musical training, sign language translation and as a rehabilitation tool for patients with hand injuries (Figure 5.a). The E-glove is essentially based on three major components: 1) VHS encapsulated CareGum sensors situated on important locomotion points on the hand, 2) a signal processing unit consisting of a wheatstone bridge for signal amplifying and a Analog to Digital Converter (ADC) that can filtrate and convert acquired data from analog to digital format, and 3) A microcontroller for handling data flow and data transfer to a PC (Figure 5.a). In an elegant example, we have utilized E-glove as a simple proto-type sign language translation device as demonstrated in Figure 5.b. Here, we have utilized five different channels – each of them covering the motion of a specific finger. Evidently, the E-glove is capable of discerning a number of signs including stop, ok, victory, strength and the numbers one and three by utilizing various five channels. Next we proceeded to demonstrate one of the first ever built cybernetic extensions with self-healing capacity (Figure 5.c). In Figure 5.c photographic images of the cybernetic E-glove in the stop, ok, impaired and self- ok and stop configuration are matched with their associated ADC signals in a custom-built PC program. Notably, from Figure 4.c a record-breaking self-healing in multicomponent electronics at 10s is observed; a record until now held at 100s by a recently developed multifunctional electronic skin system at Stanford University.[30] Even though self-healing electronics have been around for some years; in this study, we have brought this concept to an even more advanced stage heralding the promise of robust or perhaps even unbreakable consumer electronics.

Ionic conductive hydrogels have been rapidly picked up by engineers to fuel great advances in soft ionotronics. Especially, the unique combination of soft hydrogel-like materials with stretchability, transparency and ionic conductivity have given rise to a number of exciting applications including, electronic displays, artificial skin, optoelectronics and strain sensors; thereby encouraging their usage in flexible bioelectronics for real-time healthcare monitoring and user empowerment.[31] However, adhesion, self-healing and 3D printing capacity is properties needed of such sensors before customized and personalized wearable's can see the light of day. Materials displaying such galaxy of properties are definitely going to soar in the coming years, not only as components in future bionics but also generally speaking in the fields of material science, engineering and electronics. In this study we have used the beautiful marriage between silk (Si), Calcium (Ca^{+2}) tannic acid (TA) and reduced graphene oxide (rGO) to uncover such exciting materials. We coined the material CareGum and demonstrated that it could outperform most conventional systems in terms of self-healing rate (few seconds), toughness (13.9 ±2.2 MJ m^{-3}), elongation (30000 %) and multifunctionality. Generally speaking, most self-healing soft materials display low fracture toughness – typically in the kJ/m^{-3} range and heal completely only after several hours.[32] We speculate that the observed incredible CareGum toughness stem from the hierarchal crosslinking scheme behind it. This is a similar mechanism as the one observed in natural materials including bone, nacre, mussels and wood; wherein a palette of bonding types ranging from hydrogen and weak electrostatic bonds can act as a counteractive measure against crack formation to stronger covalent bonds capable of ensuring a stable and long-standing structural form.[33] The rapid self-healing time is on the other hand most likely caused by the plethora of dominant hydrogen bonds present within the CareGum matrix as their characteristic formation rate is appreciable faster than that of other self-healing cross-links including hydrophobic, electrostatic and dynamic covalent bonds.[34]

In conclusion, we envision that CareGum-based ionotronics can be implemented in applications covering robotics, cybernetics, bionics, cyborganics, wearable electronics and implantable devices. Indeed; many of todays wearable electronics and robots use hard and rigid components that restrict locomotion freedom and limits device durability. As an example, the performance of conventional exoskeletons are currently compromised by dangling wires, bulky microprocessors

and fragile electronics. Moreover, despite the fact flexible and tough electrically materials are slowly gaining momentum in this direction only few of the reported materials used in these systems encompass one of the most important requirements of living tissues, namely the ability to heal on demand in the event of injury or damage. In this study, we have demonstrated that the CareGum covers all of these bases in a hitherto unprecedented manner. Importantly, they also bode well for mass production as they are manufactured through a simple "design-mixing" procedure of non-toxic and readily available components. Indeed, the production price of CareGum is 140 USD/kg (< 3000 sensors) and the production time is less than an hour; making them easier to prepare for various commercial exploits, unlike some of their current rivals in the field.

Materials and Methods

Extraction of silk fibroin

Bombyx mori silk cocoons were obtained from Wild Fibres, UK. Silk fibroin was extracted by boiling 10 g of sliced cocoons 4L of aqueous solution containing 0.02 M sodium carbonate (Sigma-Aldrich) for 30 minutes in order to remove sericin. The extracted fibroin was washed several times with Milli-Q (MQ) water and dried at room temperature. Subsequently, the fibers were dissolved in 9.3 M lithium bromide (Honeywell) at 60 °C for 6 hours and dialyzed against MQ water for 3 days. Finally, the fibroin solution was centrifuged at 12000 rpm at 4 °C for 20 minutes (three times) to remove any impurities. The concentration of the silk fibroin in the solution was typically in the range of 6-7% w/v (60-70 mg/mL). The obtained silk fibroin solution were stored at 4 °C and consumed within 2 weeks to avoid protein denaturation

Preparation of reduced Graphene oxide (GO)

Graphene oxide (GO) was synthesized by modified Hummer's method using graphite flakes (Sigma-Aldrich, cat #332461, 150 μm flakes). In this method, 3.0 g of graphite flakes was mixed with a 9:1 mixture of concentrated H_2SO_4/H_3PO_4 (360:40 mL, Sigma-Aldrich) and stirred for 30 minutes. Then, 18.0 g of $KMnO_4$ powder (Sigma-Aldrich) was gradually added into the solution under constant stirring. The reaction was performed under an ice bath in order to prevent an exothermic reaction. After addition of $KMnO_4$, the reaction mixture was heated up to 55 °C and stirred for 3

days. Finally, the reaction mixture was cooled to room temperature and poured onto 400 mL ice. Afterwards 30% H_2O_2 was added dropwise under constant stirring until the color of the mixture turned yellow and stirred overnight at room temperature. The reaction mixture was centrifuged for 30 minutes at a speed of 13000 rpm, and solid GO was collected from the bottom. The resulting solid material was washed 3 times with 0.1 M HCl and several times with MQ water until the pH of the supernatant was 5-6. Finally, the collected solid GO material was freeze-dried and used for reduced graphene oxide preparation. In order to reduce the graphene oxide, 300 mg of freeze dried GO was dissolved in 50 ml MQ water and sonicated for 90 minutes to obtain a uniform brown solution. Then, 400 mg of Tannic Acid in 50 ml MQ water was added into the GO solution and sonicated again for 90 minutes. Finally, the reaction mixture was heated at 85 oC for 9 hours. The resulting solid material was then washed with 40 mL of MQ water and freeze-dried for 12 hours.

Preparation of Silk-reduced Graphene oxide (SiGo) supramolecular polymer compositions

Initially, stock solutions of 50% w/v tannic acid (TA, Sigma-Aldrich), 2M $CaCl_2$ and 2 mg/mL rGO were prepared. Required volumes of silk fibroin solution and $CaCl_2$ were measured and mixed together to reach a final content of 560 mg and 0.1 M, respectively. Subsequently, required volumes of graphene solutions (16, 33 and 70 mL) were mixed with the above mixture in order to reach a silk to graphene ratio of 5, 10 and 20% w/w, while the total volume was maintained at 80 mL by adding water. Finally, 5.6 ml of 50% w/v TA solution was gradually added to a stirring solution and mixed with spatula until a gum-like material appeared. Samples were washed several times with MQ water before analysis.

Scanning electron microscopy (SEM)

The SEM images of the CareGum compositions were taken by a FEI Quanta 200 ESEM FEG Scanning Electron Microscope (USA) with a field emission gun, wherein the accelerating voltage was kept at 5 kV and emission current at 5 mA. Prior to the SEM imaging the freeze dried samples were cut and sputter coated with gold (5nm) by Quorum coater Q150T (Quorum Technologies, UK).

Fourier transform infrared (FTIR) spectroscopy analysis

To evaluate the chemical interactions in the composites and structural changes of the silk fibroin, FTIR analysis were conducted using a PerkinElmer Spectrum 100 FTIR spectrometer (USA) attenuated total reflectance (ATR) mode. Data were collected at 25 oC between 4000 - 500 cm^{-1} for 16 scans at a resolution of 4 cm^{-1}. The absorbance spectra in 1580-1800 cm^{-1} range where deconvoluted using Origin 2019 software (USA), in order to determine secondary structures of silk proteins. In detail, the absorption spectra were baseline-corrected and fitted using the PeakFit routine function of Origin software with Gaussian-like peaks with a half-bandwidth of 25 cm^{-1}. The peaks corresponding to TA (C-C bond and C=O) were eliminated and the compositions of secondary structures of silk fibroin were calculated.

Thermogravimetric analysis (TGA)

TGA of the freeze-dried samples was performed using TGA Q500 Thermogravimetric analyzer (TA Instruments, USA). The mass loss of the samples were monitored as function of temperature from 30 to 900 °C with a rate of 10 °C/min under a constant nitrogen flow at 60 mL/min.

Differential Scanning Calorimetry (DSC)

DSC of the freeze-dried samples was carried out using DSC Q200 (TA Instruments) between 25 to 260 °C at a scan rate of 10 °C/min under a constant nitrogen flow of 50 mL/min. In order to acquire DSC spectra's, 3-4 mg of the samples were sealed in a Tzero aluminium pans (Switzerland) and the heat flow change is measured as a function of temperature with reference to an empty pan.

Mechanical Properties

Mechanical properties of the CareGum compositions were assessed with an Instron 5967 Universal Testing Systems (UK) in tensile and compression mode with a 500 N load-cell and the stress−strain curve was recorded using Bluehill 3 testing software. To perform the tensile measurements, molded and flattened specimens of CareGums with 22 mm length, 14 mm width and approximately 1 mm thickness were prepared. Samples were strained at a rate of 100 mm min^{-1} by keeping 2 mm gauge length until the failure point was reached. The thickness of each strip was measured independently using a digital electronic Vernier caliper before the test. For cyclic tensile measurements, the specimens were stretched up to 30% strain and in both loading and

unloading cycles, the stretching was assessed at the rate of 10 mm min-1 by keeping 5 mm gauge length. The thickness of each strip was measured independently using a digital electronic Vernier caliper before the test. The area between the loading and unloading curves for each cycle was calculated and reported as energy dissipated per unit volume. To perform the compression test, CareGum samples were molded into cylindrical shapes of 10 mm diameter and 5mm height. Samples were compressed at the rate of 0.5 mm min^{-1} until 70% compression was achieved.

Water content measurements

In order to determine the water content, the CareGum samples were freeze-dried for 24 hours and the weight of the samples was measured before (Wo) and after (Wd) freeze drying using a weighing balance with an accuracy of 0.001g. The water content (%) was subsequently calculated using the following equation:

$$\text{Water Content (\%)} = \frac{W_o - W_d}{W_o} \times 100$$

Adhesion studies

Lap shear strength experiments were used to determine the adhesive properties of CareGum on porcin skin, heart and muscle surfaces, following a standard lap-shear test method (ASTM F2255) using Instron 5967 Universal Testing Systems (UK) in tensile mode with 500 N load-cell. Tissue samples with dimensions of 10 mm x 40 mm were adhered onto CareGum samples (10 mm x 10 mm) and immersed in 37˚C PBS with 100 g weight applied during 10 minutes before testing. Similarly, the adhesive properties of CareGum samples were measured on the surface of steel, brass and glass sheet with a bonding area of 12.7 mm x 25.4 mm. The adhesion strength (Lap shear strength) was calculated as the maximum load divided by the bond area in kilo-Pascals (kPa).

Rheological analysis

Rheological characterization of CareGum compositions were conducted by using a Discovery Hybrid Rheometer HR-2, TA Instruments. Samples were loaded between two 20 mm diameter parallel plates with a 1 mm gap size at 25°C. Dynamic thermo-analysis was conducted by performing upwards and downward temperature ramps

from 15 °C to 60°C at a constant angular frequency (50 rad/s) and 1% strain. Apparent viscosity of the CareGum compositions as a function of shear rate in the range between 0.1-100 s^{-1} was measured at 25 °C. Shear storage modulus (G′) and loss modulus (G") as a function of frequency were measured with a logarithmic sweep of frequency range between 0.01-1000 rad/s at 1% strain. Shear storage modulus (G′) and loss modulus (G″) as a function of oscillation strain were measured oscillation tests with a logarithmic sweep of oscillation strain range between 0.001-100 % at 1 rad/s frequency.

Melt Spinning

To produce the melt spun fibers, the CareGum composites were filled inside a plastic syringe with nozzle size of 1 mm and heated up to 60 oC. The fibers were then extruded into water bath at 60 oC and cooled immediately after extrusion in order to keep a smooth fiber structure.

Screen Printing

To perform screen-printing of CareGum composites, patterns were created on a 0.5 mm thick plastic sheet (screen/mesh) by laser-cut using an Epilog laser-cutting machine. The patterned meshes were fixed on a flat surface (PMMA plastic) and the CareGum composites were screen printed using a squeegee blade after heating the samples at 60 oC for 10 minutes.

Ionic conductivity

Electrochemical Impedance Spectroscopy (EIS) was performed to measure the ionic conductivity of the CareGum samples using PalmSens 4 (USA). EIS spectra was recorded with an AC amplitude voltage of 10 mV in the range 100 kHz to 10 Hz. Specifically, CareGum samples (1 cm2) were sandwiched between two stainless steel plates and the recorded Nyquist data was fitted using inbuilt software to determine the solution resistance (R_s). The ionic conductivity (σ) of the samples was calculated according to the following equation:

$$\sigma = \frac{1}{R_s} \times \frac{l}{a}$$

where l and a are the thickness of the sample.

Resistance Measurements

The impedance of the CareGum sensor circuit was monitored with an Agilent 4294A precision impedance analyzer (USA) operated at 2 kHz by applying an AC voltage ranging from -0.5 to 0.5 V. To measure the resistance changes during stretching, bending or twisting, a sensor was fabricated by connecting tin plated copper sheets to both ends of 5 mm-wide, 3mm length and 1 mm thick CareGum rectangular strip. All sensors were encapsulated in an acrylic foam tape (3M VHB) to prevent the evaporation of water. At least 3 samples were measured and reported the average values.

Self-healing electronic circuit

To further demonstrate the self-healing feature of the CareGum compositions, an electronic circuit was designed consisting of a LED bulb (3-3.2V working load), CareGum as a conductor and four 9V batteries. The LED bulb was connected to the batteries through the CareGum conductor using copper wires.

Sensor for monitoring the body movements

In order to monitor the movements of the body, a sensor was fabricated by connecting tin plated copper sheets to both ends of a 5 mm-wide and 1 mm thicker CareGum rectangular strip. The length of the sensor varied from 3 to 6 cm and was attached on various moving parts of the body such as finger, wrist, forehead, hand muscle, shoulder, elbow, backhand, and knee. All sensors were encapsulated in an acrylic foam adhesive tape (3M VHB) to prevent water evaporation. The resistance changes in response to body movements were monitored with an Agilent 4294A precision impedance analyzer (USA) operated at 2 kHz by applying an AC voltage ranging from -0.5 to 0.5 V. Relative resistance ($\Delta R/R0$) was then reported as the measured values, where ΔR is the difference between the resistance at measuring scenarios and the initial resistance (R0).

Electronic glove (E-Glove) Fabrication

Initially, five sensors for E-Glove with SiGo-20% (3mm length) were fabricated as described in the previous section. Then sensors were encapsulated with double sided acrylic foam adhesive tape (3M VHB) and attached to each fingers of the SafeCut HPPE Knit Glove, Nitrile Palm by positioning the moving joint of the finger. In order

to fix the position, each end of the sensors were firmly attached to the glove by cyanoacrylate glue. Afterwards, the sensors are connected to a balanced Wheatstone bridge configuration. Any change in sensor length will result in a change in its electrical resistance, thereby bringing the bridge out of balance proportionally to the measured strain. This imbalance is then fed into a high-precision differential analog-to-digital converter. An Arduino is used to translate and transfer the data between the acquisition circuit and a computer, where a Python script configures the ADC and data acquisition parameters. These data are then presented illustratively by mapping each sensor to a finger on a three-dimensional hand model. The on-screen hand thereby moves in tandem with the measured strain signals.

Acknowledgements:

ADP would like to acknowledge the Danish Council for Independent Research (Technology and Production Sciences, 8105–00003B), the Villum Foundation (10103) and the VIDI research programme with project number R0004387, which is (partly) financed by the Netherlands Organisation for Scientific Research (NWO).

References

[1] D. N. Rockwood, R. C. Preda, T. Yücel, X. Wang, M. L. Lovett, D. L. Kaplan, Nature protocols 2011, 6, 1612; Z. Shao, F. Vollrath, Nature 2002, 418, 741.

[2] Y. Cheng, L.-D. Koh, D. Li, B. Ji, M.-Y. Han, Y.-W. Zhang, Journal of the Royal Society Interface 2014, 11, 20140305; S. Keten, Z. Xu, B. Ihle, M. J. Buehler, Nature materials 2010, 9, 359.

[3] D. Umuhoza, F. Yang, D. Long, Z. Hao, J. Dai, A. Zhao, ACS Biomaterials Science & Engineering 2020, 6, 1290; T. B. Aigner, E. DeSimone, T. Scheibel, Advanced Materials 2018, 30, 1704636; D. H. Kim, J. Viventi, J. J. Amsden, J. L. Xiao, L. Vigeland, Y. S. Kim, J. A. Blanco, B. Panilaitis, E. S. Frechette, D. Contreras, D. L. Kaplan, F. G. Omenetto, Y. G. Huang, K. C. Hwang, M. R. Zakin, B. Litt, J. A. Rogers, Nature Materials 2010, 9, 511; R. Wu, L. Ma, C. Hou, Z. Meng, W. Guo, W. Yu, R. Yu, F. Hu, X. Y. Liu, Small 2019, 15, 1901558.

[4] Y. L. Kong, M. K. Gupta, B. N. Johnson, M. C. McAlpine, Nano Today 2016, 11, 330.

[5] C. H. Yang, Z. G. Suo, Nature Reviews Materials 2018, 3, 125.

[6] B. Tulachan, S. K. Meena, R. K. Rai, C. Mallick, T. S. Kusurkar, A. K. Teotia, N. K. Sethy, K. Bhargava, S. Bhattacharya, A. Kumar, Scientific reports 2014, 4, 5434; D. Porter, F. Vollrath, Soft Matter 2013, 9, 643; N. Amdursky, E. D. Głowacki, P. Meredith, Advanced Materials 2019, 31, 1802221; X. Fu, Y. Jewel, Y. Wang, J. Liu, W.-H. Zhong, The Journal of Physical Chemistry Letters 2016, 7, 4304.

[7] P. Dubey, S. Murab, S. Karmakar, P. K. Chowdhury, S. Ghosh, Biomacromolecules 2015, 16, 3936.
[8] N. Drnovšek, R. Kocen, A. Gantar, M. Drobnič-Košorok, A. Leonardi, I. Križaj, A. Rečnik, S. Novak, Journal of Materials Chemistry B 2016, 4, 6597.
[9] K. S. Kim, Y. Zhao, H. Jang, S. Y. Lee, J. M. Kim, K. S. Kim, J.-H. Ahn, P. Kim, J.-Y. Choi, B. H. Hong, nature 2009, 457, 706; S. Bae, H. Kim, Y. Lee, X. Xu, J.-S. Park, Y. Zheng, J. Balakrishnan, T. Lei, H. R. Kim, Y. I. Song, Nature nanotechnology 2010, 5, 574.
[10] C. Lee, X. Wei, J. W. Kysar, J. Hone, science 2008, 321, 385.
[11] A. Lokhande, I. Qattan, C. D. Lokhande, S. P. Patole, Journal of Materials Chemistry A 2020, 8, 918; J. W. Suk, R. D. Piner, J. An, R. S. Ruoff, ACS nano 2010, 4, 6557.
[12] K. Ghosal, K. Sarkar, ACS Biomaterials Science & Engineering 2018, 4, 2653; S. J. Kim, K. Choi, B. Lee, Y. Kim, B. H. Hong, Annual Review of Materials Research 2015, 45, 63; X. Li, L. Zhi, Chemical Society Reviews 2018, 47, 3189; T. T. Tung, M. J. Nine, M. Krebsz, T. Pasinszki, C. J. Coghlan, D. N. Tran, D. Losic, Advanced Functional Materials 2017, 27, 1702891; N. H. Othman, M. C. Ismail, M. Mustapha, N. Sallih, K. E. Kee, R. A. Jaal, Progress in Organic Coatings 2019, 135, 82.
[13] H. Fan, L. Wang, X. Feng, Y. Bu, D. Wu, Z. Jin, Macromolecules 2017, 50, 666.
[14] T. Steiner, Angewandte Chemie-International Edition 2002, 41, 48.
[15] P. Zhou, X. Xie, D. P. Knight, X.-H. Zong, F. Deng, W.-H. Yao, Biochemistry 2004, 43, 11302.
[16] F. B. Kadumudi, M. Jahanshahi, M. Mehrali, T. G. Zsurzsan, N. Taebnia, M. Hasany, S. Mohanty, A. Knott, B. Godau, M. Akbari, A. Dolatshahi-Pirouz, Advanced Science 2019, 6.
[17] J. L. Yarger, B. R. Cherry, A. Van Der Vaart, Nature Reviews Materials 2018, 3, 1.
[18] Y. Liu, M. Pharr, G. A. Salvatore, ACS nano 2017, 11, 9614; M. Ha, S. Lim, H. Ko, Journal of Materials Chemistry B 2018, 6, 4043; R. Cao, X. Pu, X. Du, W. Yang, J. Wang, H. Guo, S. Zhao, Z. Yuan, C. Zhang, C. Li, ACS nano 2018, 12, 5190.
[19] H. Fan, J. Wang, Q. Zhang, Z. Jin, ACS Omega 2017, 2, 6668; H. Fan, J. Wang, Z. Jin, Macromolecules 2018, 51, 1696.
[20] C. Das, P. D. Olmsted, Philosophical Transactions of the Royal Society A: Mathematical, Physical and Engineering Sciences 2016, 374, 20150126; L. Coderch, O. López, A. de la Maza, J. L. Parra, American journal of clinical dermatology 2003, 4, 107; E. Fuchs, Annual review of cell and developmental biology 1995, 11, 123.
[21] T. M. Jacobson, K. Ü. Yüksel, J. C. Geesin, J. S. Gordon, A. T. Lane, R. W. Gracy, Journal of investigative dermatology 1990, 95, 296; A. V. Rawlings, I. R. Scott, C. R. Harding, P. A. Bowser, Journal of investigative dermatology 1994, 103, 731.
[22] J. Wintterlin, M.-L. Bocquet, Surface Science 2009, 603, 1841; A. Dong, Q. Fu, M. Wei, X. Bao, Applied Surface Science 2017, 412, 262.
[23] C. H. Li, C. Wang, C. Keplinger, J. L. Zuo, L. Jin, Y. Sun, P. Zheng, Y. Cao, F. Lissel, C. Linder, X. Z. You, Z. A. Bao, Nature Chemistry 2016, 8, 619.
[24] J. Kang, D. Son, G. J. N. Wang, Y. Liu, J. Lopez, Y. Kim, J. Y. Oh, T. Katsumata, J. Mun, Y. Lee, Advanced Materials 2018, 30, 1706846.

[25] S. Zhang, L. Cai, W. Li, J. Miao, T. Wang, J. Yeom, N. Sepúlveda, C. Wang, Advanced Electronic Materials 2017, 3, 1700067.
[26] J. Ramírez, B. Polat, D. J. Lipomi, ACS omega 2020; J. Wang, C. Lu, K. Zhang, Energy & Environmental Materials 2020, 3, 80; W. A. D. M. Jayathilaka, K. Qi, Y. Qin, A. Chinnappan, W. Serrano-García, C. Baskar, H. Wang, J. He, S. Cui, S. W. Thomas, Advanced Materials 2019, 31, 1805921.
[27] J. Qi, P. Yang, A. Waraich, Z. Deng, Y. Zhao, Y. Yang, Journal of biomedical informatics 2018, 87, 138; G. V. Angelov, D. P. Nikolakov, I. N. Ruskova, E. E. Gieva, M. L. Spasova, in *Enhanced Living Environments*, Springer, 2019, 226.
[28] E. Brown, H. M. Jaeger, Reports on Progress in Physics 2014, 77, 046602.
[29] C. Ramon, P. H. Schimpf, J. Haueisen, BioMedical Engineering Online 2006, 5, 10.
[30] D. Son, J. Kang, O. Vardoulis, Y. Kim, N. Matsuhisa, J. Y. Oh, J. W. F. To, J. W. Mun, T. Katsumata, Y. X. Liu, A. F. McGuire, M. Krason, F. Molina-Lopez, J. Ham, U. Kraft, Y. Lee, Y. Yun, J. B. H. Tok, Z. N. Bao, Nature Nanotechnology 2018, 13, 1057.
[31] L. Fan, J. Xie, Y. Zheng, D. Wei, D. Yao, J. Zhang, T. Zhang, ACS Applied Materials & Interfaces 2020, 12, 22225; Y. Zhou, C. Wan, Y. Yang, H. Yang, S. Wang, Z. Dai, K. Ji, H. Jiang, X. Chen, Y. Long, Advanced Functional Materials 2019, 29, 1806220; C. Yang, Z. Suo, Nature Reviews Materials 2018, 3, 125; C. Keplinger, J. Y. Sun, C. C. Foo, P. Rothemund, G. M. Whitesides, Z. G. Suo, Science 2013, 341, 984; X. Jing, H.-Y. Mi, Y.-J. Lin, E. Enriquez, X.-F. Peng, L.-S. Turng, ACS applied materials & interfaces 2018, 10, 20897.
[32] C. B. Rodell, N. N. Dusaj, C. B. Highley, J. A. Burdick, Advanced materials 2016, 28, 8419; A. Jahandideh, N. Moini, K. Kabiri, M. J. Zohuriaan-Mehr, Chemical Engineering Journal 2019, 370, 274.
[33] H. Zhao, Z. Yang, L. Guo, NPG Asia Materials 2018, 10, 1; H. Qu, H. Fu, Z. Han, Y. Sun, RSC advances 2019, 9, 26252; R. Ajdary, B. L. Tardy, B. D. Mattos, L. Bai, O. J. Rojas, Advanced Materials 2020, 2001085.
[34] S. Talebian, M. Mehrali, N. Taebnia, C. P. Pennisi, F. B. Kadumudi, J. Foroughi, M. Hasany, M. Nikkhah, M. Akbari, G. Orive, Advanced Science 2019, 6, 1801664.

Figure 1

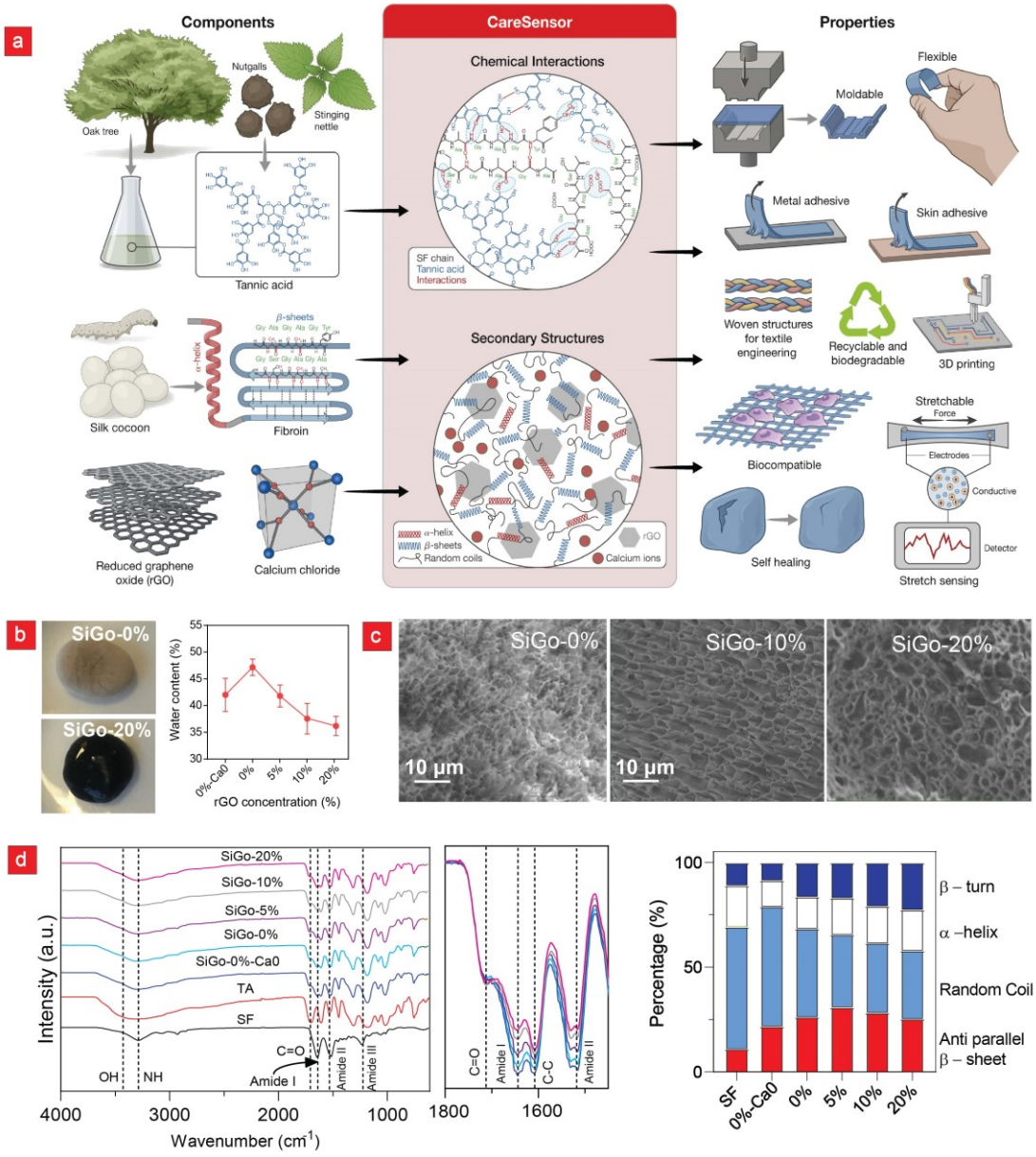

Figure 1. Fabrication of CareGums and their characterization. **(a)** The components used for preparation of CareGums are shown here together with the chemical interactions giving rise to them and their various material properties. **(b)** The photographic images of composites without and with 20% rGO. **(c)** Cross-section SEM images of the composites showing their intricate matrix pore structures. **(d)** FTIR spectra of pristine components and composites - with enlarged FTIR spectra of the 1800 and 1450 cm^{-1} to region. (e) The secondary structure composition of the various compositions.

Figure 2

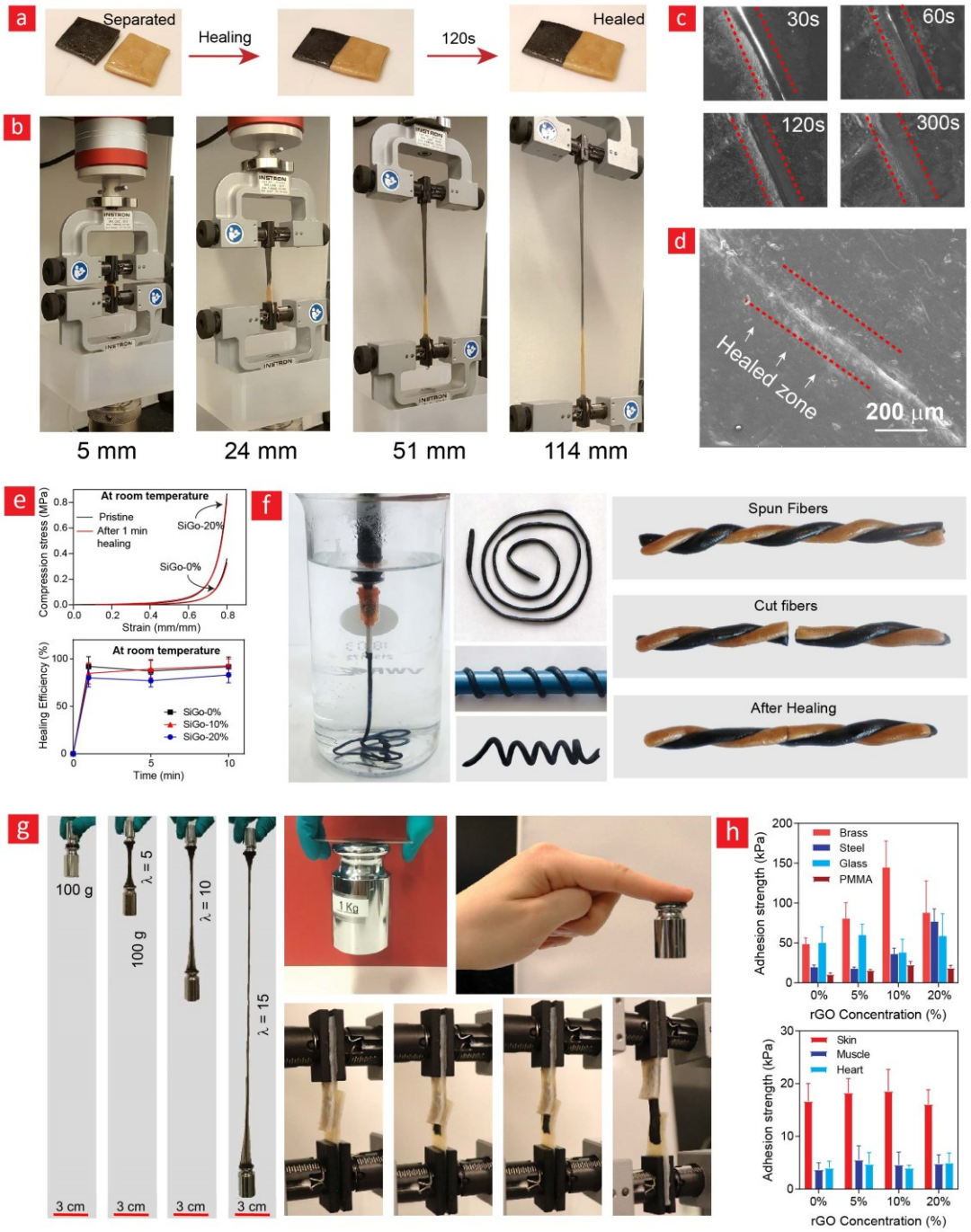

Figure 2. CareGum self-healing, weaving and adhesion properties. (a) Photographic images showing the self-healing ability of CareGum. **(b)** Mechanical stretching of self-healed composites. **(c)** Optical Microscopic images of the self-healing of SiGo-20% composites at different time intervals. **(d)** SEM images of the SiGo-20% composites after 5 min healing **(e)** Compression stress-strain curve of SiGo-0% and SiGo-20% composites before and after 1 min self-healing and self-healing efficiency calculated after 1, 5 and 10 min.. **(f)** Textile-like fibers produced by melt spinning are showed here together with their twisting, and self-healing ability. (g) The cohesive adhesion of SiGo-20% on stainless steel, glass, human skin are put on display here together with lap-shear measurements on porcine skin, (h) Comparison of CareGum adhesion strength on different surfaces as measured from lap-shear test.

Figure 3

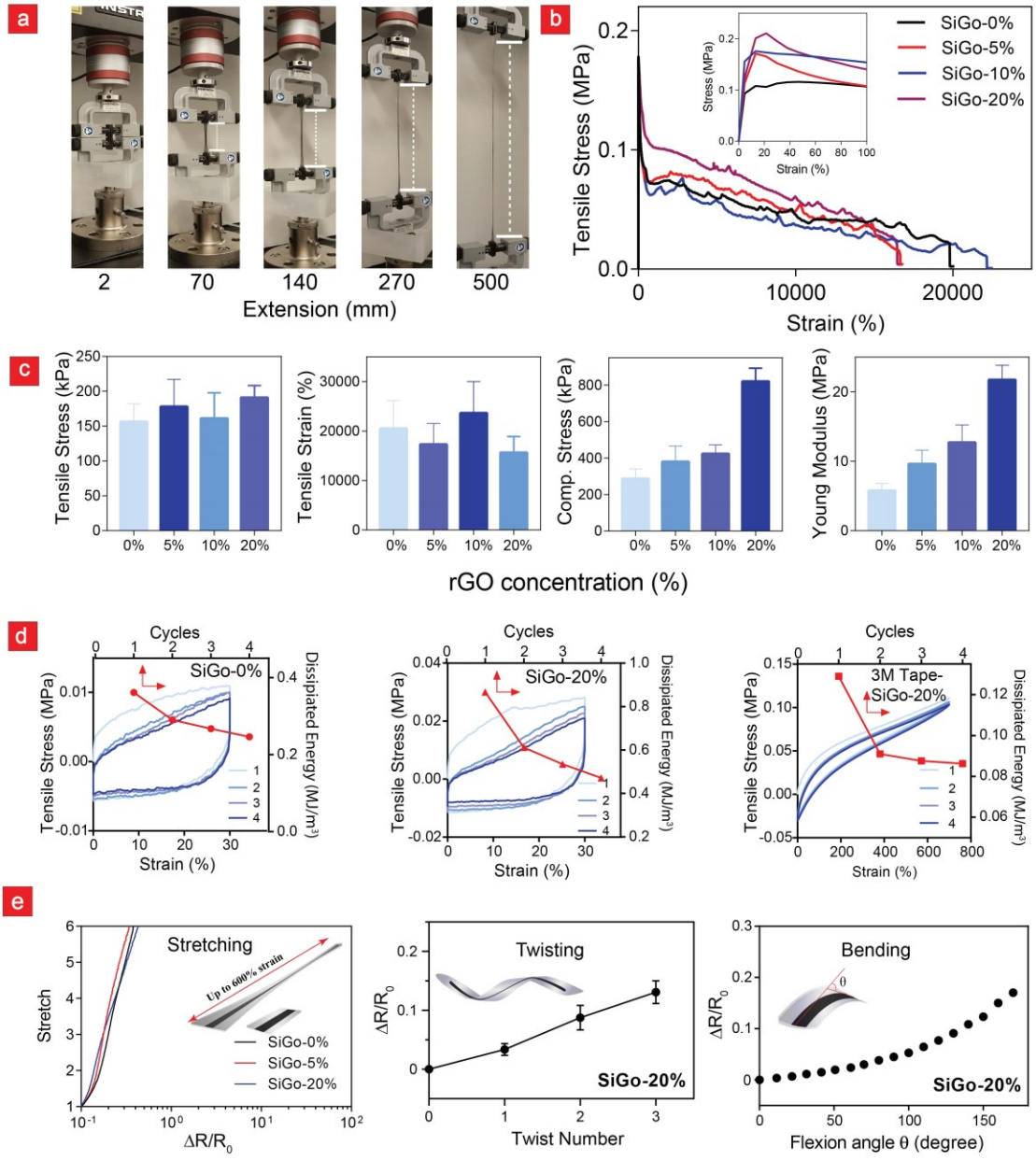

Figure 3. Mechanical analysis. **(a)** Photographic images showing the tensile stretching of CareGums with Instron mechanical tester. **(b)** Typical tress-strain curve of the composites. **(c)** The maximum stress, and strain values from tensile analysis and compression stress and young modulus values are displayed here after. **(d)** Four successive cycle loading-unloading of tensile curve for SiGo-0% and SiGo-20 % until 30% strain, and SiGo-20% encapsulated in a 3M VHB tape until 600% are shown here. The corresponding dissipation energy calculated for each cycle is also depicted in the graph. **(e)** Normalized electrical impedance of the composites as function of stretch were compared and normalized electrical impedance in percentage as a function of bending and twisting for SiGo-20% were measured and put on display here.

Figure 4

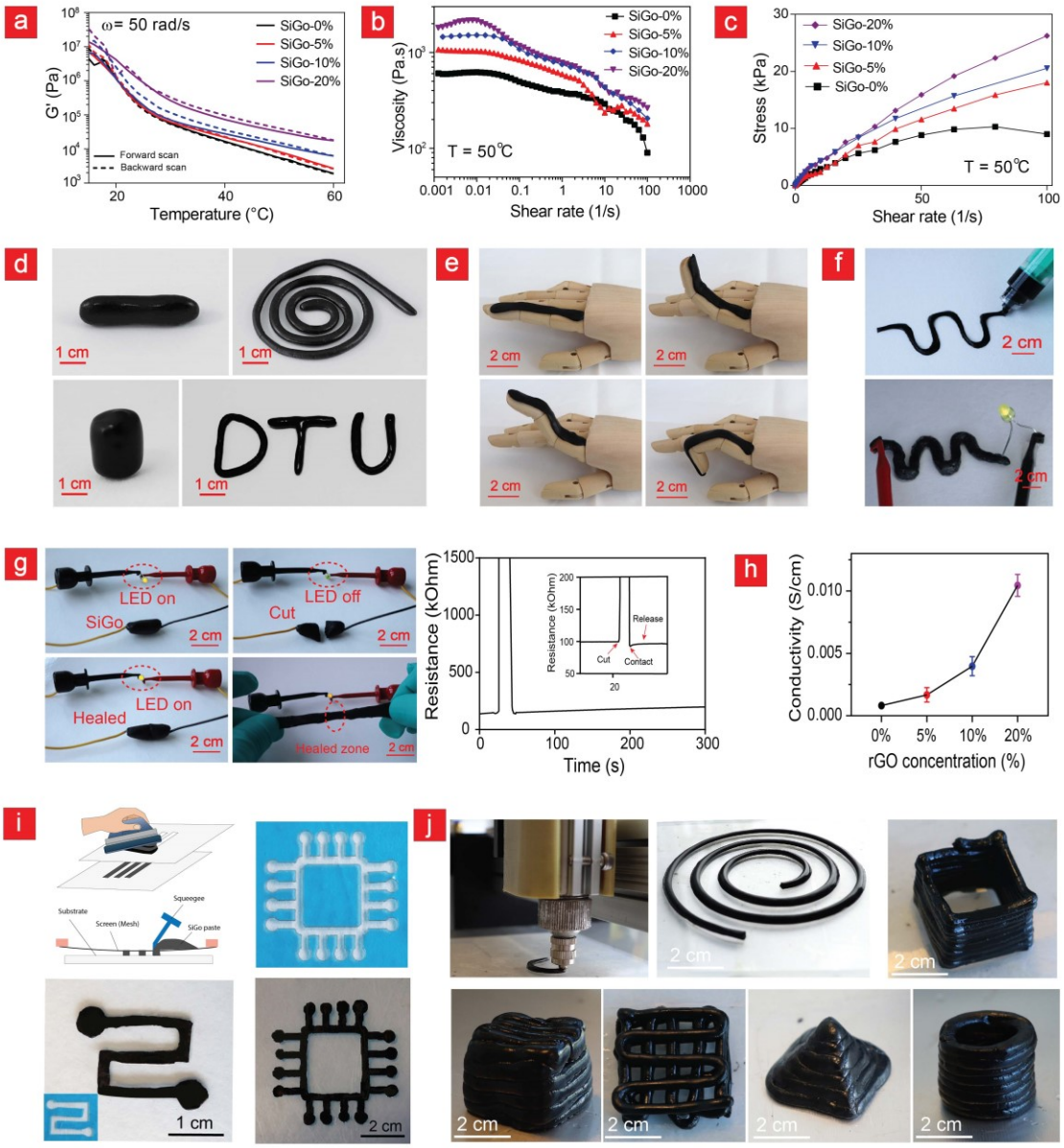

Figure 4. CareGum rheology and printability. Rheological properties including **(a)** storage modulus as function of temperature, **(b)** viscosity as a function of shear rate, and **(c)** stress as a function of shear rate. Photographic images **(d)** demonstrating moldability, **(e)** conformability and **(f)** injectability of the SiGO-20% composites. **(g)** A CareGum circuit showing a turned on LED lamp that can self-heal after breakage and even keep shinning after the healed parts have been stretched. **(h)** Ionic conductivity of as function of rGO concentration as calculated from the impedance measurements. **(i)**The generation of complex 2D printed structures via CareGum using screen printing. **(j)** CareGum are also printable into complex 3D structure through extrusion printing.

Figure 5

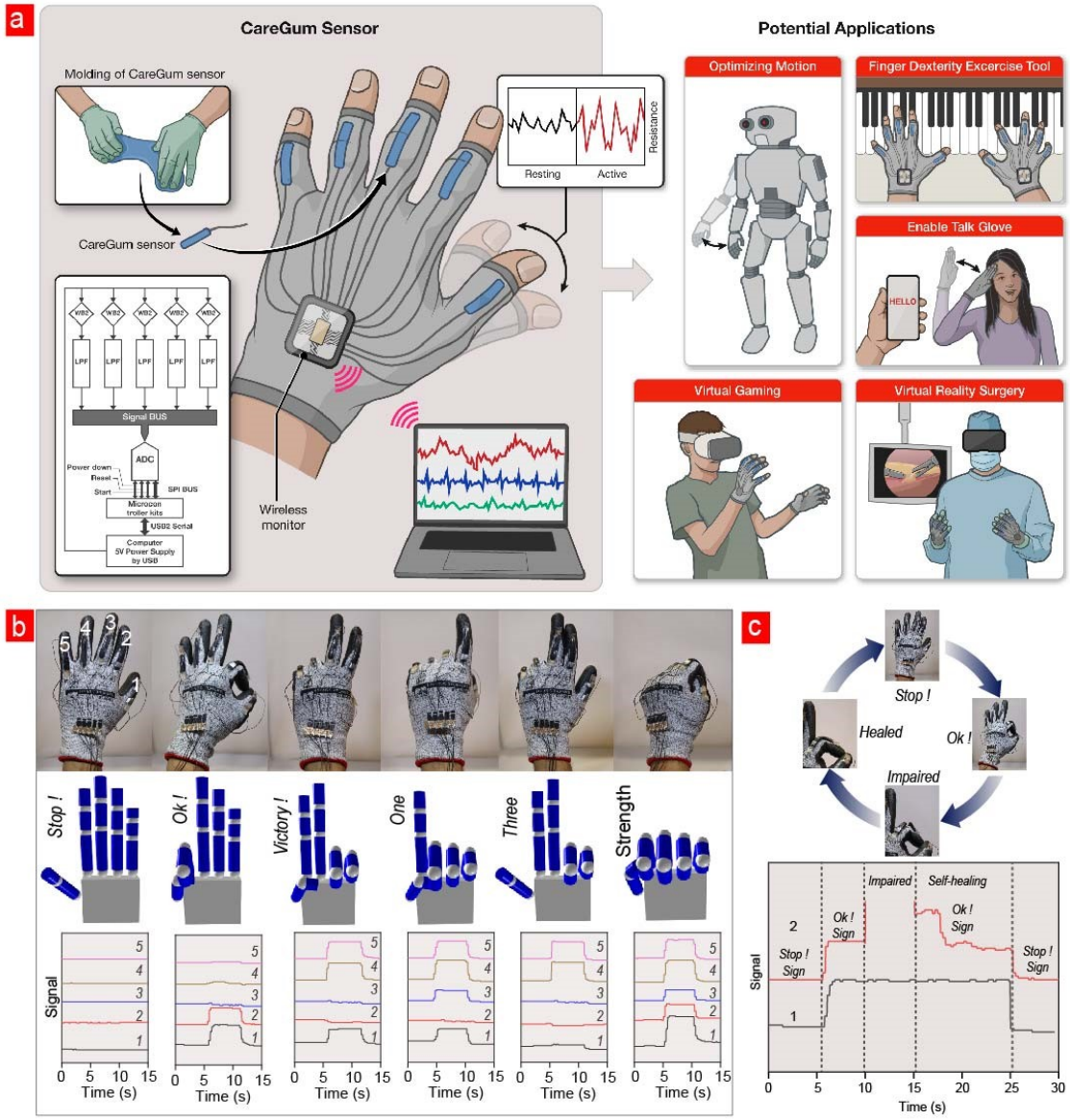

Figure 5. Sensing hand gesture with a self-healable Bionic E-glove. (a) Schematic diagram showing the E-glove fabrication and its potential applications. **(b)** Photos showing hand gesture with E-glove and corresponding images of the virtual hand in different positions and the associated signal responses from five fingers (five channels). (**c)** Photos showing different hand gestures with E-glove – both in an impaired and self-healed state - and their corresponding signal changes.